

THE UV PROPERTIES OF
POST-STARBURST QUASARS

By

Allison Leigh Strom

A Thesis Submitted to The Honors College
In Partial Fulfillment of the Bachelors Degree
With Honors in
Physics

THE UNIVERSITY OF ARIZONA

May 2010

Approved by:

Philip Pinto
Department of Physics

STATEMENT BY AUTHOR

I hereby grant to the University of Arizona Library the nonexclusive worldwide right to reproduce and distribute my thesis and abstract (herein, the licensed materials), in whole or in part, in any and all media of distribution and in any format in existence now or developed in the future. I represent and warrant to the University of Arizona that the licensed materials are my original work, that I am the sole owner of all rights in and to the licensed materials, and that none of the licensed materials infringe or violate the rights of others. I further represent that I have obtained all necessary rights to permit the University of Arizona Library to reproduce and distribute any nonpublic third party software necessary to access, display, run, or print my thesis. I acknowledge that the University of Arizona Library may elect not to distribute my thesis in digital format if, in its reasonable judgment, it believes all such rights have not been secured.

Signed: _____

Abstract

Observations have revealed a class of objects that simultaneously exhibit evidence for a quasar and a massive, luminous, moderately-aged starburst ($\sim 10^{10} M_{\odot}$ and ~ 100 Myr). These post-starburst quasars (PSQs) may be an important link in the evolutionary history of galaxies, providing insight into the transformation from young, blue, early-type star-forming galaxies to older, red, late-type quiescent galaxies. Although studies of composite objects like PSQs have become more common, surveys with the *Galaxy Evolution Explorer* (*GALEX*) provide a unique opportunity to study a statistically significant population at wavelengths underutilized in the literature. For our sample, we have spectroscopically-selected 609 PSQs from SDSS DR3 based on the strength of the Balmer jump and the $H\delta$ absorption line. Here, we report on the methods used to conduct FUV and NUV photometric measurements for the 529 objects observed by *GALEX* and present the first results, including *GALEX*-SDSS colors. We also discuss the status of ongoing work using *GALEX* photometry to explore the overall UV properties of post-starburst quasars and consider the use of UV excesses to probe the existence of young stars (as young as several Myr old) formed after the starburst.

Contents

1	Introduction	5
1.1	Black Hole-Galaxy Coevolution	5
1.2	Post-Starburst Quasars	5
2	Data	7
2.1	Sample Selection	7
2.2	The Galaxy Evolution Explorer	7
2.3	UV Imaging	10
3	UV Photometry	12
3.1	Aperture Corrections	14
4	Results	16
4.1	UV Colors	16
4.2	Connection with the Optical	16
5	Future Work	20
5.1	Complementary Samples	20
5.2	FUV and NUV Flux Excesses	20
5.3	Stacking of Non-detections	20
	References	22

1 Introduction

1.1 Black Hole-Galaxy Coevolution

For the past decade, evidence for an “AGN-starburst” connection has grown, and studies of these composite objects have been performed at multiple wavelengths to try and disentangle the relationship between black hole growth and star formation. Essentially every large galaxy harbors a black hole of $\sim 0.15\%$ the mass of its spheroidal component (e.g., Gebhardt et al. 2000), but theorists (e.g., Burkert & Silk 2001) are still trying to understand whether the black hole or stars form first (or whether they grow together) and how both processes may regulate each other.

Prompted by the discovery of ultraluminous infrared galaxies (ULIRGs: $L_{\text{IR}} > 10^{12}L_{\odot}$), strongly interacting mergers with contributions from both starburst and AGN power sources, Sanders et al. (1988) hypothesized that these galaxies evolve into normal blue quasars after the central engine clears away the dust associated with the massive star formation. The relative numbers of ULIRGs and quasars support this interpretation, and observations in the far-infrared produce some objects which might be candidates for a transitional stage (Stockton 1999). However, conclusive evidence of a connection between ULIRGs and their supposed-quasar descendants has yet to be found, and some groups report results that conflict with the Sanders picture of galaxy evolution. Boyce et al. (1996) suggest that the IRAS-selected quasars are the products of *young* spiral mergers, not advanced mergers, and Genzel et al. (1998) conclude that the presence of an AGN is not correlated with merger advancement.

Observations in the ultraviolet lag behind those in the infrared, where the most energetically star-forming galaxies are often identified. Although there are studies of both AGN activity and star formation rates in the UV, direct comparisons between the two are not commonly seen in the literature. Because the UV is rich with indicators of star formation and emission from the central engine, the primary task when studying composite objects becomes one of separating the competing contributions from the two sources.

1.2 Post-Starburst Quasars

Post-starburst quasars (PSQs) are objects that show simultaneous emission from an AGN and a massive luminous starburst ~ 100 Myr old, with composite spectra displaying broad emission lines as well as the Balmer jumps and strong Balmer absorption lines characteristic of type-A stars. The prototypical PSQ is UN J1025 – 0040

(Brotherton et al. 1999), which exhibits evidence of a massive starburst component ~ 400 Myr old with a bolometric luminosity ($10^{11.6} L_{\odot}$) equal to that of the quasar. Objects like UN J1025 – 0040 observed only tens of Myrs after the starburst would have a more luminous stellar population and would likely be dust enshrouded, placing them in the ULIRG class. HST WFPC2 imaging (Brotherton et al. 2002) shows that the starburst is nuclear, the host resembles a merger remnant, and a less massive young starburst is present. All of this *suggests* that UN J1025 – 0040 is a plausible transition between ULIRGs and quasars, but we require more observational evidence to evaluate whether this idea of galaxy evolution is correct. In this paper, we present the first efforts to probe the young stellar content of transition objects like UN J1025 – 0040 using observations from the Sloan Digital Sky Survey (SDSS) and the *Galaxy Evolution Explorer* (GALEX).

2 Data

2.1 Sample Selection

We spectroscopically selected PSQs from SDSS DR3 using an automated algorithm based on one used by Zabludoff et al. (1996) to select post-starburst galaxies (PSGs) using Balmer jumps and $H\delta$ absorption lines. We find 609 PSQs with $z < 0.8$ (Figure 1) that show clear evidence of post-starburst populations of significant luminosity/mass. In addition to using the spectra from SDSS, we are also interested in the g -band magnitudes, which range from 16.1 to 21.3 for our sample (Figure 2).

SDSS and HST images show that nearly 40% of the PSQs appear to be close doubles or have companions (Cales et al., in prep), and most single sources show extended fuzz or tidal features. While some PSQs are seen inhabiting spiral galaxies, others are clearly hosted by disturbed elliptical galaxies, suggesting the same correlation with major merger and post-merger systems as seen in PSGs, which are uniformly interacting systems.

2.2 The Galaxy Evolution Explorer

The *Galaxy Evolution Explorer* (*GALEX*; Martin et al. 2005; Morrissey et al. 2007) is a NASA Explorer Mission launched in early 2003. Designed to perform a UV survey of the sky from 1350-2750 Å, *GALEX* has provided an unprecedented look at the entire sky in the space ultraviolet, where signatures of star formation can be exploited to study galaxy environments. The goals of the *GALEX* mission are threefold: to provide a method of calibration for UV star formation rates (SFRs), to determine the star formation history over the lifetime of the universe from $0 < z < 2$, and to generate a statistically significant sample of nearby galaxies to correlate with multiwavelength data. In particular, there is a large amount of interest and work being done on combined *GALEX*-SDSS datasets that allow for basic source classification using UV-optical colors (e.g., Seibert et al. 2005).

The 0.5-m diameter modified Ritchey-Chrétien telescope has a wide 1.25° field of view and simultaneous imaging coverage in the FUV (1350-1750 Å) and NUV (1750-2750 Å) with a pair of photon-counting, microchannel plate, delay line readout detectors. The image resolution of the instrument is $4.2''$ in the FUV band and $5.3''$ in the NUV band. With $1.5''$ pixels, this translates to a FWHM of approximately 2.8 pixels in the FUV and 3.5 pixels in the NUV. A grism mode, intended for low-resolution spectroscopy ($\lambda/\Delta\lambda \sim 118 - 200$), is also available, but rarely used.

GALEX occupies a circular, 700 km, 29° inclination orbit, with science obser-

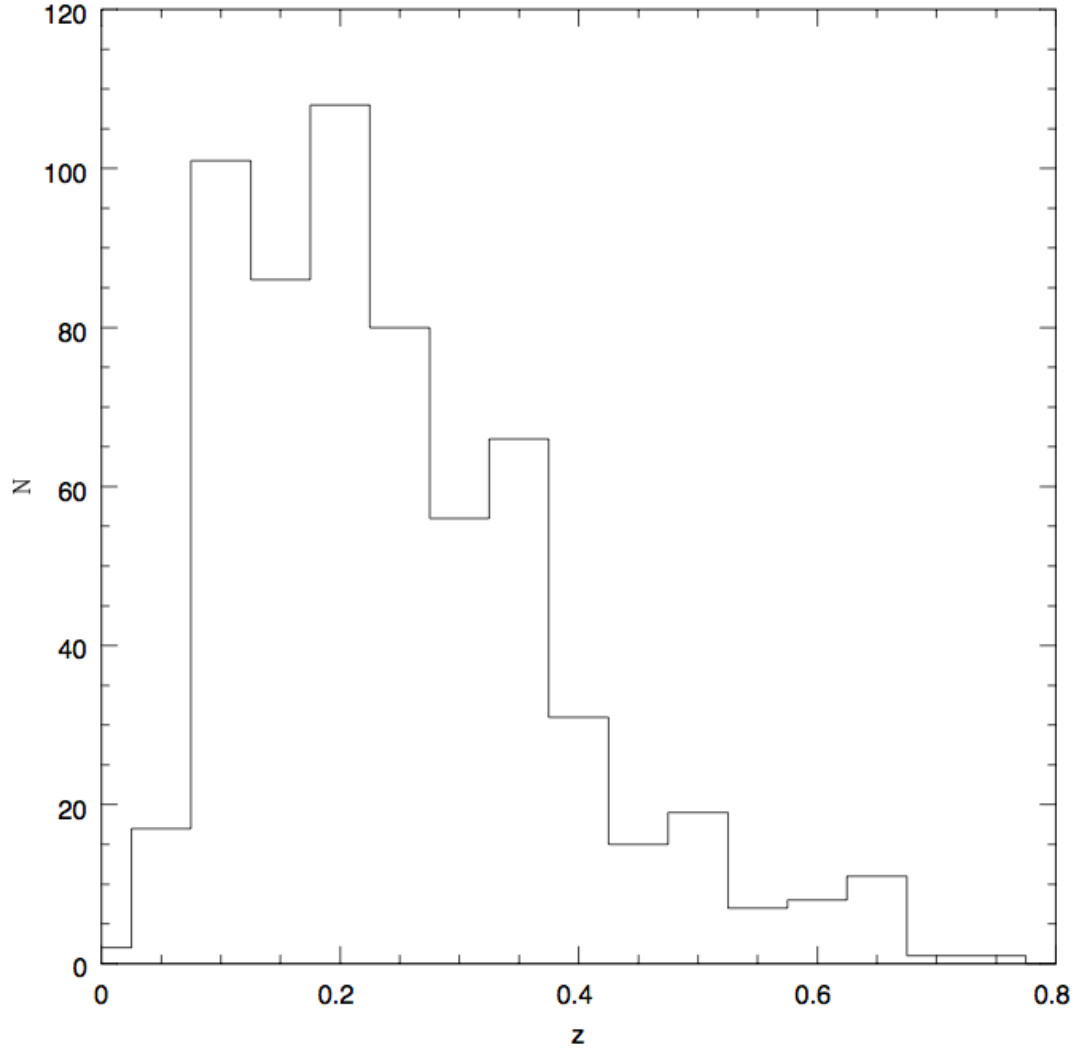


Figure 1: The redshift distribution of our 609 PSQs, a sample that represents about 5% of $z < 0.75$ quasars. Our sample is in the local universe, but this is an effect due in part to the selection criteria, which rely on the observation of characteristic features in the optical.

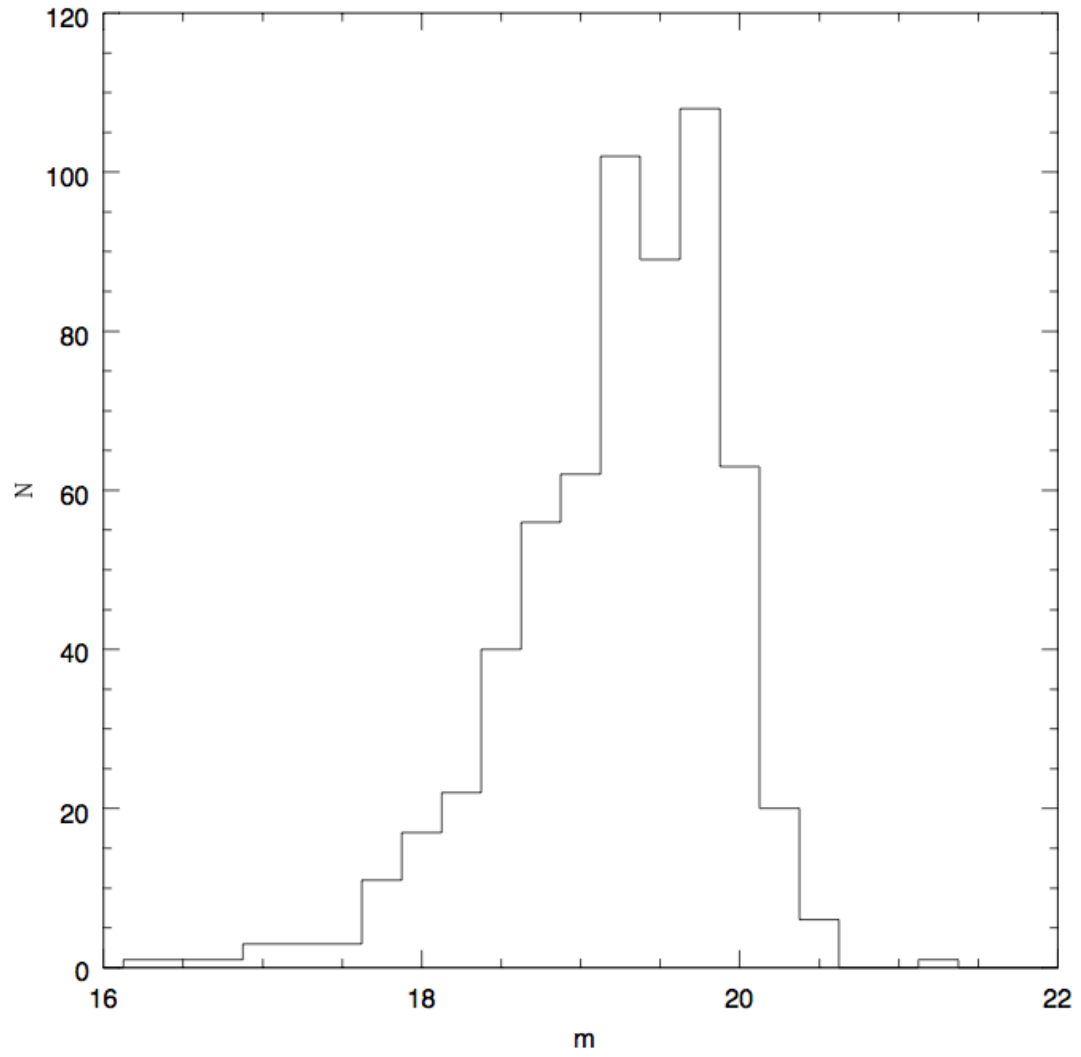


Figure 2: The g -mag distribution for the PSQ sample, which peaks at ~ 19.5 .

vations taken during the “night” segment of the orbit ($\sim 1500 - 1800$ s) to avoid background contamination from the sun. Night-sky background contamination is low, dominated by diffuse galactic light in the FUV and zodiacal light in the NUV. The detectors cannot point near the sun, earth, or bright stars, which leaves 87% of the sky accessible; if the one of the detectors is turned off, this can be extended to 95% (in the case of FUV-only observations).

The workhorse survey of the mission is the All-sky Imaging Survey (AIS), which covers some 3/4 of the sky and is sensitive to $m_{AB} \sim 21$. During each observation period, an average of 10 different fields (10 deg^2) are observed, with a typical exposure time of 100 s and several hundred to 1000 objects observed per field. The AIS was designed to complement other large surveys, primarily SDSS, and comprises the vast majority of the data products produced by the mission.

The other surveys are deeper, but restricted to smaller fractions of the observable sky. Medium Imaging Survey (MIS) exposures are a single orbit, typically 1500 s, and cover a total observed area of 1000 deg^2 with sensitivity $m_{AB} \sim 23$. The Deep Imaging Survey (DIS) consists of 20 orbit exposures (~ 30 ks, $m_{AB} \sim 25$) over 80 deg^2 and is designed to overlap with existing multiwavelength coverage.

Standard pipeline processing produces a variety of data products, with the intensity maps (-int.fits, counts $\text{s}^{-1} \text{ pixel}^{-1}$) being the most frequently used. These images are created from the raw count maps (-cnt.fits, counts pixel^{-1}), which are divided by the high-resolution relative response map (essentially the flat field times the exposure map interpolated to the same pixel scale). The intensity maps are not background subtracted. Smoothed sky background maps (-skybg.fits, counts $\text{s}^{-1} \text{ pixel}^{-1}$) are generated separately by the *GALEX* pipeline using a method that takes into account the low count rates of the background (see Morrissey et al. 2007 for a full discussion). Examples of the data products are shown in Figure 3.

2.3 UV Imaging

Only 529 of our 609 PSQs have been observed by *GALEX* and are found in 3420 separate tiles (1674 FUV, 1746 NUV), over 70% of which are from the AIS. The tiles come from the most recent releases, GR4 and GR5 (hereafter GR4/5), which contain a combination of new observations taken in 2007 and 2008 as well as reprocessed tiles from previous releases. As with all *GALEX* releases, tiles processed via the GR4/5 pipeline supersede the previous data products.

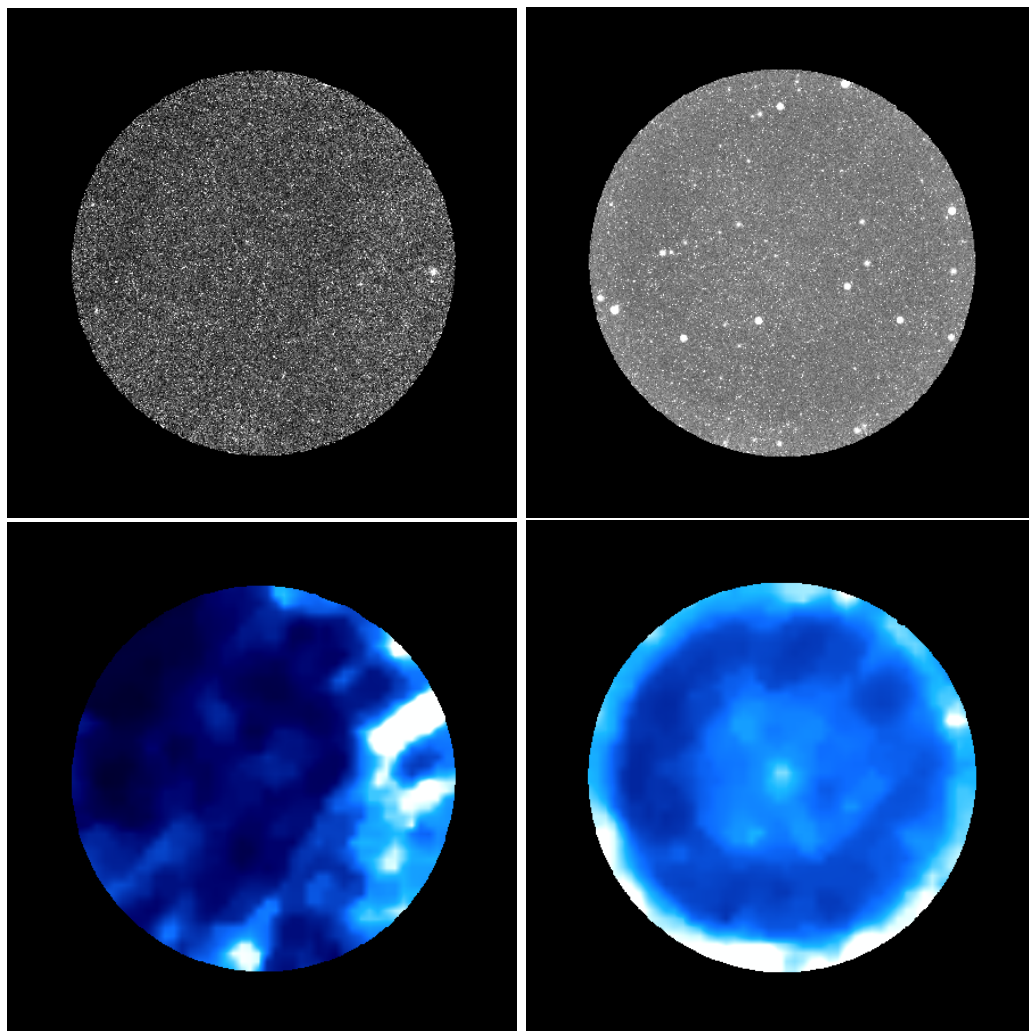


Figure 3: Images showing various data products for *GALEX* observations of WHTDF-00. Top left, FUV intensity map ($\text{counts s}^{-1} \text{ pixel}^{-1}$); top right, NUV intensity map. Bottom left, the FUV sky background map determined by the pipeline ($\text{counts s}^{-1} \text{ pixel}^{-1}$); bottom right, the NUV sky background map. Note that both the FUV and NUV background can vary with position in the field.

3 UV Photometry

Despite the ready availability of UV magnitudes from the *GALEX* data product pipeline, we chose to conduct our own photometric analysis of the PSQs independently. This was for several reasons: 1) we planned on performing the same analysis for multiple samples (PSQs, PSGs, and quasars); 2) we wanted flexibility in selecting photometric parameters; and 3) when objects are observed more than once or have more than one entry in the *GALEX* catalog, it is often unclear how to compare values from different epochs, especially if tiles have been reprocessed or are co-adds. Because the UV sky is relatively uncrowded and the PSF is sufficiently large that our objects appear as point sources, we opted for aperture photometry over modeling methods.

When using the *apphot* package in IRAF, as we did, it is important to account for exposure time of *GALEX* tiles when using the standard tasks, which assume that the images contain total accumulated counts instead of the counts-per-second in the intensity maps; multiplying tiles by their exposure time creates an image which will then be handled properly by *apphot*. Otherwise, we followed precedent and conducted our photometric analysis using the recommended values for parameters, adjusted as appropriate for the *GALEX* tiles. The photometric aperture used for all objects was $8.68''$ ($11.40''$) in the FUV (NUV), or 1σ of the PSF, and the apertures were centered on the object using a centroid fitting algorithm. In lieu of using the modeled sky background maps, we accounted for the contribution of the sky by calculating the standard deviation of the background of the intensity maps and took this as the constant background across the aperture. The zero-point magnitude for the FUV (NUV) is 18.82 (20.08).

Although, typically, the conversion from *GALEX* counts-per-second (CPS) to magnitudes in the AB system is

$$\begin{aligned} \text{FUV} : m_{\text{AB}} &= -2.5 \log(\text{CPS}_{\text{tile}}) + 18.82 \\ \text{NUV} : m_{\text{AB}} &= -2.5 \log(\text{CPS}_{\text{tile}}) + 20.08, \end{aligned}$$

we were interested in a single-valued measurement of the magnitude for each object. To this effect, we instead calculated magnitudes with a CPS_{tot} , which is the total number of counts for all of the observations divided by the total exposure time for the same observations (Figure 4).

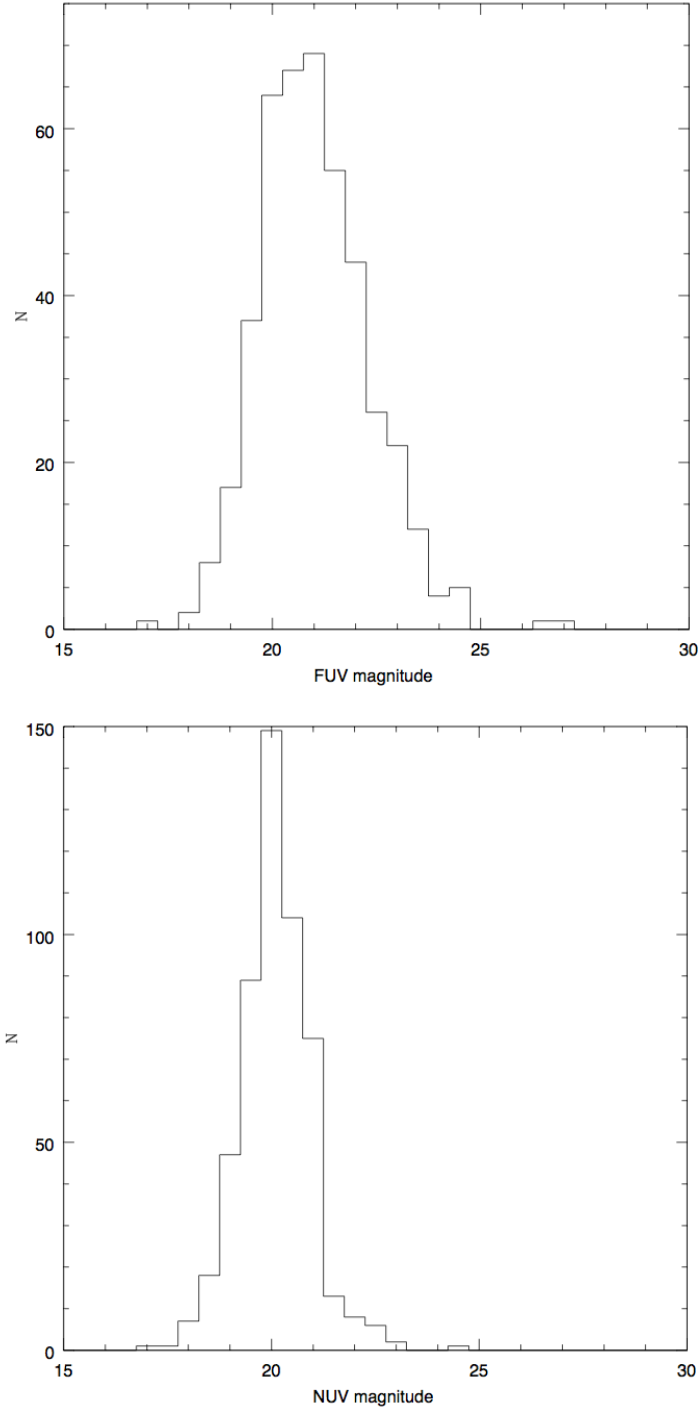


Figure 4: Magnitude distributions for the ~ 530 PSQs observed by *GALEX* in the FUV (top) and NUV(bottom). Note that the population of objects is, overall, fainter in the FUV than the NUV, suggesting that the UV emission might be being bolstered by some source (like young stars) which is brighter at longer wavelengths.

3.1 Aperture Corrections

Despite the relative sparseness of objects in the *GALEX* tiles, the occurrence of objects near enough to the PSFs to contaminate our photometry was high enough to warrant concern. To combat this issue, we chose a relatively small aperture radius and calculated aperture corrections two ways.

First, we applied a rudimentary technique by looking at the change in magnitude as a function of aperture radius for a ten hand-selected objects with uniform PSFs and no close neighbors. Using a range of apertures from 1.5''-18.0'', we found an aperture correction of ~ 1 for both bands, which was unexpectedly large.

A more sophisticated method of applying aperture corrections is to use the deepest images and look for a dependency of magnitude on aperture radius for all objects in the images. To do this, we used *daofind* to identify all of the objects in images with exposure times $> 10,000$ s and performed aperture photometry for all of them with the standard aperture (8.7'' and 11.4'') and the desired "corrected" aperture, which we took to be 18.0''. For objects that were 30'' away from any other object and were also 2 magnitudes brighter than the average background, we investigated possible structure in the aperture correction ($\Delta m = m_{\text{standard}} - m_{18''}$) as a function of magnitude and position in the field. From this method, we found that an aperture correction of $\Delta m = 0.03$ ($\Delta m = 0.04$) was appropriate for the FUV (NUV) band. Figure 5 shows the correlation between FUV and NUV magnitudes, incorporating the aperture correction for both bands.

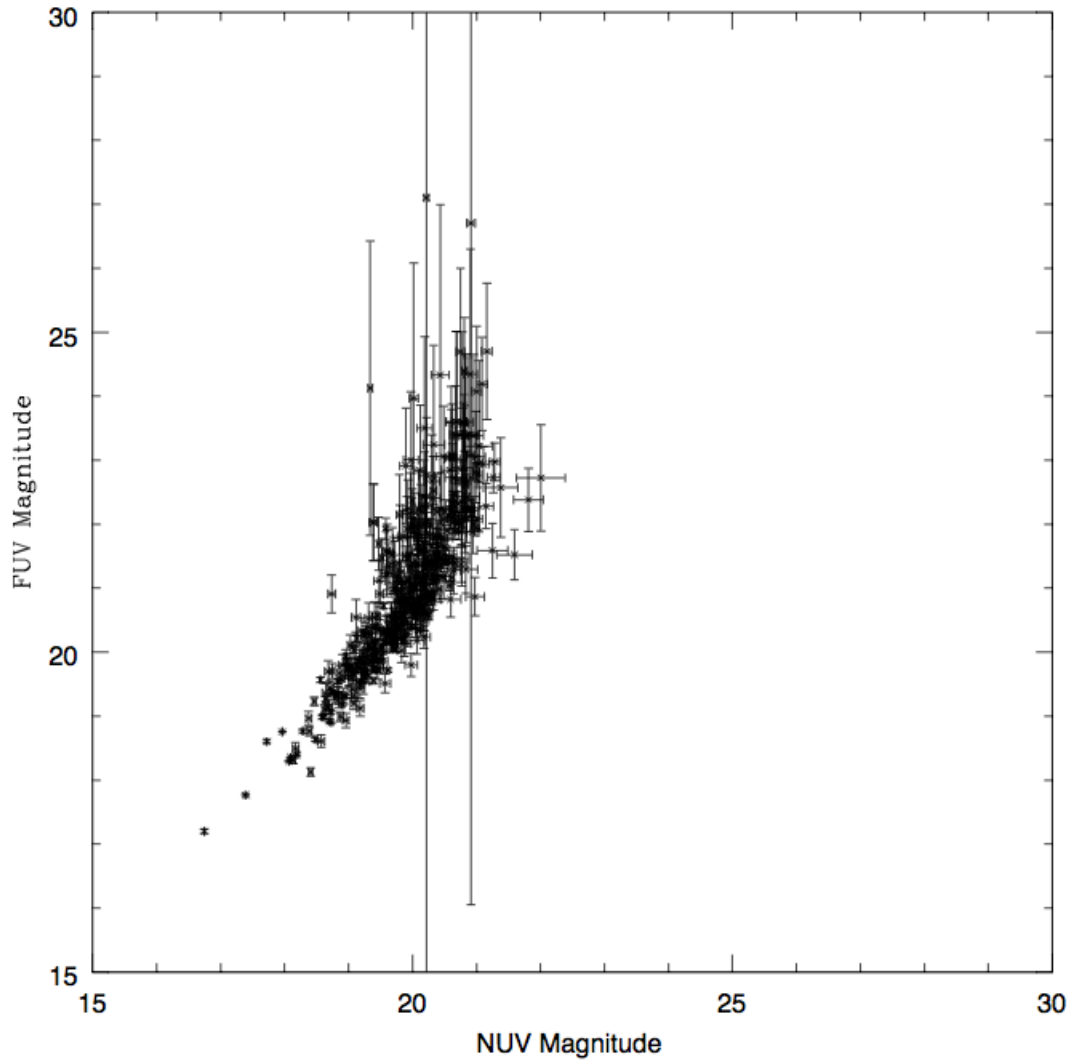


Figure 5: A plot showing FUV magnitude versus NUV magnitude for the PSQs with observations in both bands. If the UV emission were due entirely to the presence of a quasar, we might expect something like a straight line in this plot, but instead see a non-linear trend at fainter magnitudes.

4 Results

4.1 UV Colors

Figure 6 is a “color-magnitude” diagram for our sample of PSQs, showing the characteristic scatter at fainter magnitudes. The large errors for the UV colors (FUV-NUV) are due primarily to uncertainty in the FUV magnitudes, which arise due to the low number of counts observed at those wavelengths.

Regardless, there appears to be some evolution with color, with the faintest objects being much redder overall than their brighter counterparts. This might suggest that the galaxies with less total UV emission are dominated more by young stars than quasar light in these bands, since the O and B stars of a young population would contribute preferentially in the NUV.

4.2 Connection with the Optical

Although *GALEX*-SDSS colors are sometimes used in the classification of objects, Figure 7 proves inconclusive, due to the scatter in FUV-NUV color relative to NUV-g color. Regardless of UV color, the PSQs all possess relatively similar UV-optical colors. The relatively tight clustering of PSQs with NUV-g colors between 0 and 2 might be point toward physical similarities between all PSQs; however, looking at the same plot with FUV-g colors instead reveals that the same population of PSQs is very different in the FUV.

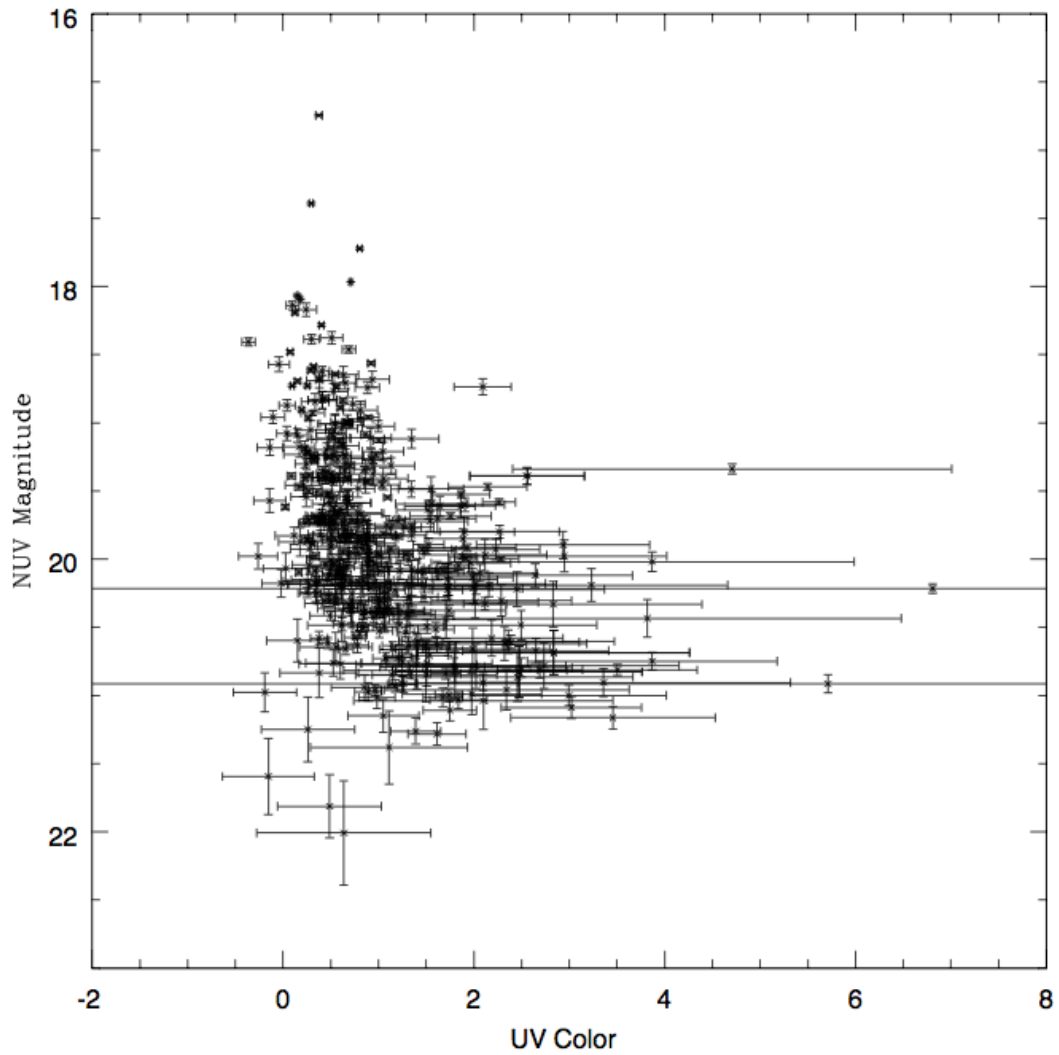


Figure 6: A “color-magnitude” diagram for the sample of PSQs observed by *GALEX*. Although the trend is somewhat obscured by increasing scatter at higher magnitudes, the faintest objects seem to be redder, overall, than the brightest galaxies. This may indicate a fundamental difference in the dominant source of UV emission between bright and faint PSQs.

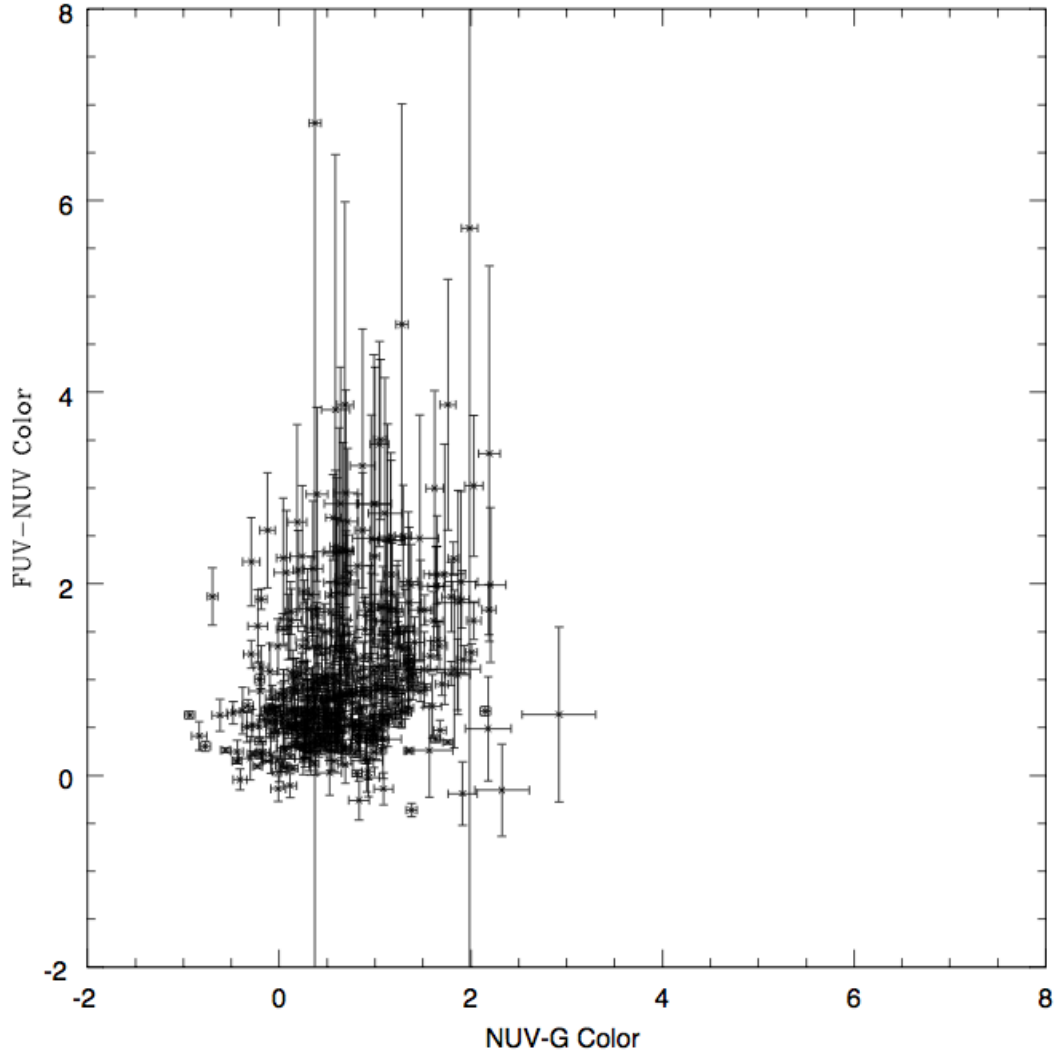


Figure 7: A traditional color-color plot for the *GALEX* PSQs, showing FUV-NUV versus NUV-g. Although similar diagnostics can be applied in differentiating between classes of objects, there seems to be little to no difference between objects within our sample.

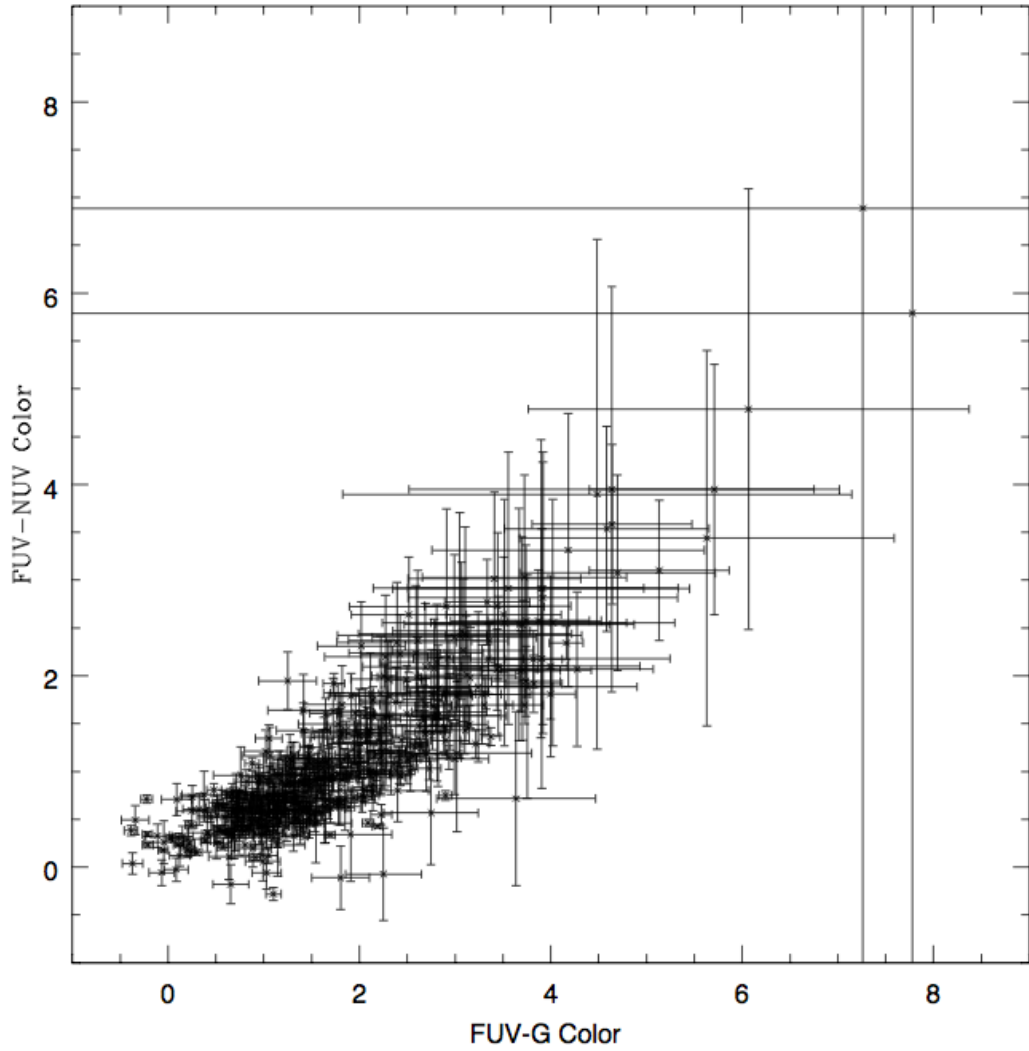


Figure 8: A traditional color-color plot for the *GALEX* PSQs, showing FUV-NUV versus FUV-g. Comparison of this figure with Figure 7 reveals an interesting difference between objects which appear largely similar in the NUV, suggesting again that the difference between emission processes in PSQs is likely to be found in the FUV.

5 Future Work

5.1 Complementary Samples

One of the most illuminating tests in considering the significance of our results will be the comparison of the UV magnitudes and colors of post-starburst quasars with complementary samples of post-starburst galaxies and ordinary quasars.

In conjunction with the photometric analysis of the PSQs by *GALEX*, we also retrieved tiles containing ~ 500 PSGs from the catalog provided by Goto (2007). Also referred to in the literature as E+A galaxies, the definition of a PSG in our sample is a galaxy with an $H\delta$ equivalent width of $> 5 \text{ \AA}$ and no detectable emission in [OII] and $H\alpha$.

For our sample of quasars, we consider all objects spectroscopically identified by SDSS as QSOs in the redshift range $0.01 < z < 0.80$, for a total of 12,488 objects. The process of obtaining photometry for those quasars in the same tiles as the PSQs and PSGs is currently ongoing.

5.2 FUV and NUV Flux Excesses

One aspect of the project which was previously done using photometry from *GALEX* data releases GR2/3 involved calculation of FUV and NUV flux excesses. To separate host galaxy flux from the quasar contribution, we adapted a method from Vanden Berk et al. (2006), who use principal component analysis to perform spectral decomposition of AGN and their host galaxies. In particular, we use the flux fractions from the host galaxies of 11,648 broad-line AGNs in the 4160-4210 \AA band to scale a quasar composite (Vanden Berk et al. 2001) to the blue end of the SDSS spectrum for each PSQ (Figure 9). We estimate flux levels in both UV bands for only the quasar using the extrapolated composite and the *GALEX* filter response functions. We hope to apply the same method to the newest UV catalog from this paper.

5.3 Stacking of Non-detections

Finally, we hope to obtain an upper limit for the average undetected PSQ by stacking *GALEX* images of non-detections in order to beat down the noise of the individual tiles. Preliminary attempts to do this have thus far yielded no results, but may prove eminently useful when the PSQ catalog is expanded to SDSS DR7.

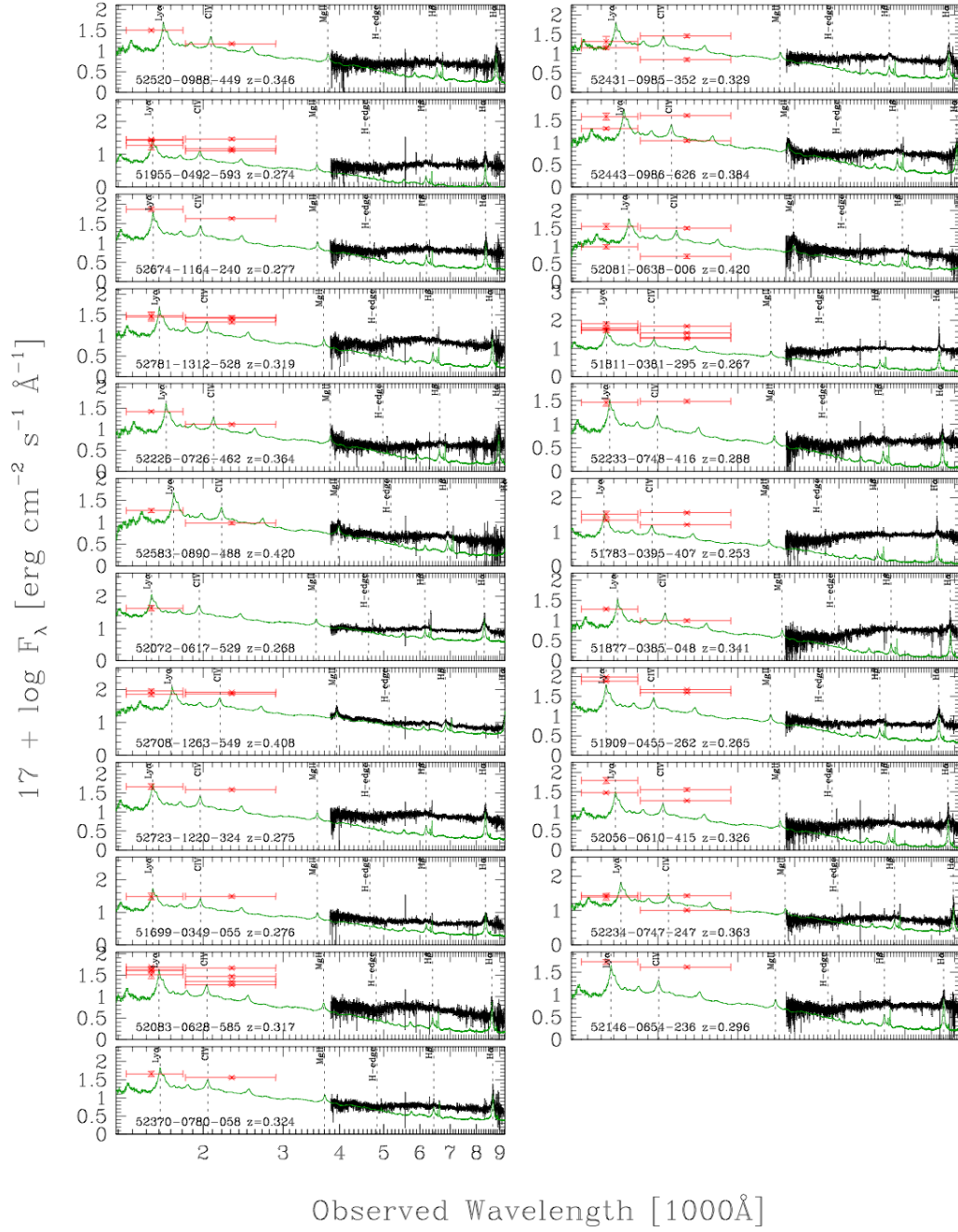


Figure 9: Spectral plots for the sample of PSQs covered by GR2/3 with corresponding HST/ACS Snapshot imaging (Cales et al., in prep). Black histogram, SDSS optical spectrum. Green histogram, scaled and extrapolated Vanden Berk quasar composite. Red points with error bars, GALEX photometry; horizontal bars indicate width of bandpass, not uncertainties.

References

- Boyce, P.J., et al. 1996, ApJ, 473, 760
- Brotherton, M. S., et al. 1999, ApJ, 520, L87
- Brotherton, M. S., et al. 2002, PASP, 114, 593
- Burkert, A. & Silk, J. 2001, ApJL, 554, L151
- Cales, S., et al., in prep.
- Gebhardt, K., et al. 2000, ApJL, 539, L13
- Genzel, R., et al. 1998, ApJ, 498, 579
- Goto, T. 2007, MNRAS, 381, 187
- Martin, D. C., et al. 2005, ApJL, 619, L1
- Morrissey, P., et al. 2007, ApJS, 173, 682
- Seibert, M., et al. 2005, ApJL, 619, L23
- Sanders, D. B., et al. 1988, ApJ, 328, L35
- Stockton, A. 1999, IAU Symp. 186: Galaxy Interactions at Low and High z , 186, 331
- Vanden Berk, D. E., et al. 2001, AJ, 122, 549
- Vanden Berk, D. E., et al. 2006, AJ, 131, 84
- Zabludoff, A. I., et al. 1996, ApJ, 466, 105